Digital Object Identifier (DOI): 10.1109/ECCE.2017.8096623

2017 IEEE Energy Conversion Congress and Exposition (ECCE), Cincinnati, OH, USA

Impacts of rotor current control targets on DC-link capacitor lifetime in DFIG-based wind turbine during grid voltage unbalance

Holger Jedtberg
Marius Langwasser
Rongwu Zhu
Giampaolo Buticchi
Marco Liserre

Suggested Citation

H. Jedtberg, M. Langwasser, R. Zhu, G. Buticchi and M. Liserre, "Impacts of rotor current control targets on DC-link capacitor lifetime in DFIG-based wind turbine during grid voltage unbalance," *2017 IEEE Energy Conversion Congress and Exposition (ECCE)*, Cincinnati, OH, 2017, pp. 3489-3495.

Impacts of Rotor Current Control Targets on DC-link Capacitor Lifetime in DFIG-based Wind Turbine during Grid Voltage Unbalance

Holger Jedtberg, Marius Langwasser, Rongwu Zhu, Giampaolo Buticchi and Marco Liserre
Chair of Power Electronics
Christian-Albrechts-Universität zu Kiel
Kiel, Germany
hje@tf.uni-kiel.de, mlan@tf.uni-kiel.de, rzh@tf.uni-kiel.de, gibu@tf.uni-kiel.de, ml@tf.uni-kiel.de

***Abstract*— In doubly-fed induction generator (DFIG)-based wind turbines, the DC-link capacitor of the back-to-back (B2B) converters is one of the components that tend to fail most often. The equivalent resistance of electrolytic capacitors is frequency dependent and presents higher values in the low-frequency range. Therefore, additional low-frequency ripple current components will stress the DC-link capacitor and reduce its lifetime. Under unbalanced grid voltage conditions, the conventional vector control strategy of the rotor side converter may be replaced by flexible multi-objective control strategies, leading to different low-frequency harmonics in DC-link capacitor current. Therefore, in this paper the differences between the different control targets with respect to overall RMS current, additional low-frequency ripple current and temperature are analyzed by means of simulations for a 2 MW DFIG wind turbine.**

Keywords*— Doubly-fed induction generator, grid faults, lifetime estimation, DC-link capacitor.

I. INTRODUCTION

In recent years, wind energy has been playing an important role in renewable power production. Wind turbine systems with doubly-fed induction generator (DFIG) are one of the most common technical solutions, due to the merits of low-scale voltage-source back-to-back (B2B) converters and flexible active and reactive power decoupling control. In B2B converters, besides film capacitors, electrolytic capacitors are often implemented in DC-link. Recent field-experiment studies showed that faults in the power electronic converters account for a great share of the overall wind turbine systems faults [1]. Moreover, capacitors are regarded as one of the weakest parts in power converters [2].

Besides ambient temperature and operating voltage, the thermal stress caused by the capacitor ripple current is considered as one of the main stressors of electrolytic capacitors [2]. The hotspot temperature is a function of the thermal resistance and the dissipated power of the capacitor, whereas the latter is the product of the square of the capacitor ripple current and the equivalent series resistance (ESR). Since the ESR of electrolytic capacitors is decreasing with frequency as discussed in [4] and [5], low frequency ripple current stresses lead to comparatively high loss fractions in the overall capacitor losses. Thus, these stress components will have a major impact on the capacitor's hotspot temperature and, therefore, studies on operating conditions that cause low frequency capacitor ripple current components need to be carried out.

The DC-link capacitor ripple current of the B2B converter depends on the control strategy as well as on the grid condition. Due to the direct grid connection of the stator, DFIG is sensitive to the grid disturbances and the DC-link of B2B-converter suffers from grid disturbances through both sides. As stated in [6], due to its volatile nature, the increasing integration of distributed renewable energy sources into the power grid leads to considerable technical challenges with respect to power quality. Among others, voltage and frequency fluctuations are considered as the most critical factors regarding grid stability. Grid-side disturbances, such as voltage sags and voltage unbalances, are expected to become more crucial affecting the connected components. Additionally, the wind power generators may be geographically located in rural areas, where the grid is relatively weak and grid voltage variations and faults frequently occur [7, 8]. Thus, the impacts of grid voltage disturbance on DC capacitor current ripples need to be studied in detail.

To deal with unbalanced voltage, the classical rotor current control strategy of the rotor side converter might be replaced by a dual-loop control strategy, as demonstrated in [9, 10] and [11], where both positive and negative sequence components of the rotor currents are controlled. With this approach different control targets might be addressed, like balanced stator currents, constant stator active power, constant stator reactive power or constant electromechanical torque. These control targets will result in different rotor current references, especially different negative sequence components. As analyzed in [12] due to negative sequence components in the rotor currents the DC-link capacitor will face additional low-frequency harmonics, that contribute to the dissipated power, heating up the capacitor and decreasing its lifetime. Therefore, special attention has to be paid to the contribution of different

rotor current control targets to low frequency ripple current stress in the DC-link in the event of unbalanced grid voltages.

In this paper, the effect of a voltage unbalance based on a negative sequence of 3% is considered for a 2 MW DFIG wind turbine system simulation study case. Although the negative sequence is often limited to 2% in many international regulations, in some specific cases a greater unbalance can happen (i.e., generator start). The negative sequence of 3% is chosen as a proof-of-concept value to better highlight the effects on the capacitors.

The paper is organized as follows. In Section II the empirical lifetime model of the electrolytic capacitor is given. The theoretical expressions of the rotor current references are derived in Section III. The simulation results for a 2 MW DFIG wind turbine study case are presented in Section IV and the impacts of the different control targets on the relative lifetime of a single DC-link capacitor are discussed. Section V concludes this paper.

II. Lifetime of Electrolytic Capacitors

A general empirical capacitor lifetime model is given by (1), where L_0 is the lifetime under test conditions as given in the data sheet, V is the operating voltage and V_0 the test voltage, n denotes a manufacturer dependent voltage stress constant, E_a is the activation energy, k_B denotes the Boltzmann constant and T_h and $T_{h,0}$ are the hotspot temperatures during use and test conditions, respectively [5], Subsequently, K_V and K_T are voltage and temperature factor, respectively.

$$L = L_0 \left(\frac{V}{V_0} \right)^{-n} 2^{\left(\frac{T_{h0} - T_h}{10K} \right)} = L_0 K_V K_T \tag{1}$$

It can be seen that lifetime is decreasing with increasing voltage and hotspot temperature. The hotspot temperature of the capacitor is dependent on the dissipated power P_d, the thermal resistance R_{th} of the capacitor, and the ambient temperature T_a and can be calculated with (2).

$$T_h = R_{th} P_d + T_a = \Delta T_h + T_a \tag{2}$$

As can be seen in (3), to respect the frequency dependence of the capacitor's ESR, the dissipated power is the sum of the product of the squared capacitor RMS ripple components $I_{c,h}$ with the respective ESR component $R_{ESR,h}$ at the corresponding frequency harmonics h of the capacitor current.

$$P_d = \sum_h I_{c,h}^2 R_{ESR,h} \tag{3}$$

The temperature factor of the lifetime model in (1) can be split into two parts. The first characterizes the impact of ambient temperature on the lifetime and is represented by the ambient temperature factor K_{Ta}, whereas by means of the second part the impact of hotspot temperature increase due to the capacitor ripple current on the lifetime can be quantified. This term is denoted by ripple current factor K_I.

$$K_T = 2^{\left(\frac{T_{h0} - T_a}{10K} \right)} 2^{\left(\frac{-\Delta T_h}{10K} \right)} = K_{Ta} K_I \tag{4}$$

In this study, the impact of different rotor current control targets on the DC-link capacitor lifetime is analyzed. In order to compare the changes in lifetime due to the control strategies it is assumed that the operating voltage as well as the ambient temperature remain constant for all cases. Therefore, the changes in lifetime are only dependent on the hotspot temperature increase due to the capacitor ripple current. Subsequently, the lifetime change with respect to the base case can be represented by means of the relative lifetime, which is the quotient of the ripple current factor of respective control target x and the ripple current factor of the base case, as given in (5).

$$L_{rel,x} = \frac{K_{I,x}}{K_{I,base}} \tag{5}$$

The capacitor under test (CUT) is an electrolytic capacitor with the data given in TABLE I. Its ESR versus frequency curve is shown in Fig. 1, where the ESR at 100Hz and 23 °C is regarded as base value. It can be seen that the ESR value is relative high in low frequency range as compared to the high frequency range. Additionally, the ESR is also affected by the temperature. The temperature dependence of the ESR is neglected in this paper.

TABLE I Data of Capacitor Under Test

Parameters		Values
Nominal Capacitance	C_{nom}	4500uF
Nominal DC voltage	V_{nom}	500V
Nominal ESR (100 Hz)	$R_{ESR,\,nom}$	21.1mΩ
Thermal Resistance	R_{th}	2.9K/W
Can dimensions	(D*L)	90mm*98mm

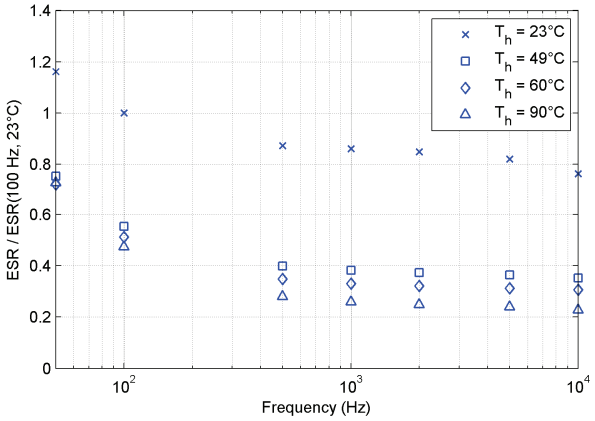

Fig. 1 Measured ESR versus frequency curve of the CUT at different hotspot temperature levels

III. Muliti-Objectives Control of Rotor Side Converter

A typical system configuration of a wind turbine with DFIG is shown in Fig. 2(a). In order to study the impacts of rotor control objectives, the DFIG model and the considered

control objectives during balanced and unbalanced grid conditions are explained in a simplified form in this part based on [9] and [11]. In Fig. 2(b) the structure of the multi-objective rotor current control is presented.

A. Balanced grid voltage

During grid voltage balanced conditions, in the synchronous rotating reference frame, the stator flux, power and electromagnetic torque can be expressed as,

$$\begin{cases} \varphi_{sd} = L_s i_{sd} + L_m i_{rd} \\ \varphi_{sq} = L_s i_{sq} + L_m i_{rq} \end{cases} \tag{6}$$

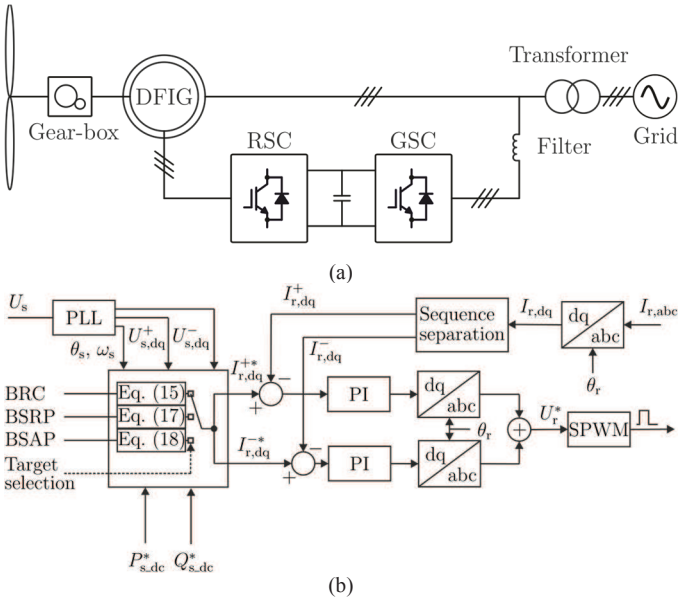

Fig. 2 Wind turbine with DFIG: (a) Typical system configuration; (b) Structure of multi-objective rotor current control.

$$\begin{cases} P_s = 1.5\left(u_{sd} i_{sd} + u_{sq} i_{sq}\right) \\ Q_s = 1.5\left(u_{sq} i_{sd} - u_{sd} i_{sq}\right) \end{cases} \tag{7}$$

$$T_e = -1.5 n_p \left(\varphi_{sq} i_{rd} - \varphi_{sd} i_{rq}\right) \tag{8}$$

By aligning all parameters with stator flux vector and substituting (6) into (7) to replace the stator current with the rotor current and stator flux, the stator active and reactive power can be expressed as,

$$\begin{cases} P_s = -1.5 u_{sq} \dfrac{L_m i_{rq}}{L_s} \\ Q_s = 1.5 u_{sq} \dfrac{\varphi_{sd} - L_m i_{rd}}{L_s} \end{cases} \tag{9}$$

In (9), it depicts that the stator active and reactive power can be regulated by controlling the rotor q- and d-axis current, respectively. This is the basic control for the DFIG, when the grid voltage is assumed balanced.

B. Unbalanced grid voltage

During unbalanced grid voltage conditions, a negative sequence component will occur and change the system performances. Therefore, the effects of the grid voltage on DFIG performance need to be considered.

When the grid voltage is unbalanced, the stator voltage and flux include positive and negative sequence components.

$$\begin{cases} u_{sdq} = u^+_{sdq} + u^-_{sdq} \\ \varphi_{sdq} = \varphi^+_{sdq} + \varphi^-_{sdq} \end{cases} \tag{10}$$

where superscripts "+" and "-" represent the positive and negative sequence component, respectively, "s" represents the stator variable, "d" and "q" represent the d- and q-axis variable, respectively.

Then, the stator active and reactive power can be expressed as,

$$\begin{cases} P_s = P_{s\_dc} + P_{s\_c2} + P_{s\_s2} \\ Q_s = Q_{s\_dc} + Q_{s\_c2} + Q_{s\_s2} \end{cases} \tag{11}$$

On the right hand side of (11), the first term is the DC component of the power, the second and third terms are the second-order disturbances.

$$\begin{vmatrix} P_{s\_dc} \\ Q_{s\_dc} \\ P_{s\_s2} \\ P_{s\_c2} \\ Q_{s\_s2} \\ Q_{s\_c2} \end{vmatrix} = -\frac{3}{2\omega_s L_s} \begin{vmatrix} 0 & 0 & 0 & 0 \\ u^+_{sq+} & -u^+_{sd+} & u^-_{sq-} & -u^-_{sd-} \\ u^-_{sq-} & -u^-_{sd-} & -u^+_{sq+} & u^+_{sd+} \\ u^-_{sd-} & u^-_{sq-} & u^+_{sd+} & u^+_{sq+} \\ 0 & 0 & 0 & 0 \\ 0 & 0 & 0 & 0 \end{vmatrix} \begin{vmatrix} u^+_{sq+} \\ -u^+_{sd+} \\ -u^-_{sq-} \\ u^-_{sd-} \end{vmatrix} + \frac{3L_m}{2L_s} \begin{vmatrix} u^+_{sd+} & u^+_{sq+} & u^-_{sd-} & u^-_{sq-} \\ u^+_{sq+} & -u^+_{sd+} & u^-_{sq-} & -u^-_{sd-} \\ u^-_{sq-} & -u^-_{sd-} & -u^+_{sq+} & u^+_{sd+} \\ u^-_{sd-} & u^-_{sq-} & u^+_{sd+} & u^+_{sq+} \\ -u^-_{sd-} & -u^-_{sq-} & u^+_{sd+} & u^+_{sq+} \\ u^-_{sq-} & -u^-_{sd-} & u^+_{sq+} & -u^+_{sd+} \end{vmatrix} \begin{vmatrix} i^+_{rd+} \\ i^+_{rq+} \\ i^-_{rd-} \\ i^-_{rq-} \end{vmatrix} \tag{12}$$

where the subscripts "+" and "-" represent the positive and negative sequence synchronous rotating reference frame.

Similarly, the electromagnetic torque can be expressed as,

$$T_e = T_{e\_dc} + T_{s\_c2} + T_{s\_s2} \tag{13}$$

Similar to (11), on the right hand side of (13), the first term is the DC component of the torque, the second and third terms are the second-order disturbances.

$$\begin{vmatrix} T_{e\_dc} \\ T_{e\_c2} \\ T_{e\_s2} \end{vmatrix} = \frac{3L_m}{2L_s}\frac{n_p}{\omega_r}\begin{vmatrix} u_{sd+}^{+} & u_{sq+}^{+} & -u_{sd-}^{-} & -u_{sq-}^{-} \\ -u_{sd-}^{-} & -u_{sq-}^{-} & u_{sd+}^{+} & u_{sq+}^{+} \\ -u_{sq-}^{-} & u_{sd-}^{-} & -u_{sq+}^{+} & u_{sd+}^{+} \end{vmatrix}\begin{vmatrix} i_{rd+}^{+} \\ i_{rq+}^{+} \\ i_{rd-}^{-} \\ i_{rq-}^{-} \end{vmatrix} \tag{14}$$

Compared to (7) and (8), where the stator power and electromagnetic torque only include the positive sequence components and, thus, are balanced, the stator active and reactive power as well as electromagnetic torque in (12) and (13) include second-order distortions.

C. Multi-objective control

a) Balanced rotor current (BRC)

In this case, the reference of negative sequence rotor current is equal to zero, and then based on (9) the rotor current reference can be obtained as,

$$\begin{vmatrix} i_{rd+}^{+} \\ i_{rq+}^{+} \\ i_{rd-}^{-} \\ i_{rq-}^{-} \end{vmatrix} = \begin{vmatrix} \dfrac{P_{s\_dc\_ref}L_s}{1.5u_{sq+}^{+}L_m} \\ \dfrac{\varphi_{sd}}{L_m} - \dfrac{Q_{s\_dc\_ref}L_s}{1.5u_{sq+}^{+}L_m} \\ 0 \\ 0 \end{vmatrix} \tag{15}$$

b) Balanced stator reactive power and electromagnetic torque (BSRP)

Comparing (12) with (14), it can be obtained that,

$$Q_{s\_s2} = \frac{\omega_r}{n_p}T_{e\_c2}\,,\ Q_{s\_c2} = -\frac{\omega_r}{n_p}T_{e\_s2} \tag{16}$$

Therefore, balanced stator reactive power and electromagnetic torque can be obtained simultaneously. In this case, the reactive power oscillation terms are set to zero, and then the reference current can be obtained as,

$$\begin{vmatrix} i_{rd+}^{+} \\ i_{rq+}^{+} \\ i_{rd-}^{-} \\ i_{rq-}^{-} \end{vmatrix} = \frac{1}{\omega_s L_m}\begin{vmatrix} u_{sq+}^{+} \\ -u_{sd+}^{+} \\ -u_{sq-}^{-} \\ u_{sd-}^{-} \end{vmatrix} + \frac{2}{3}\frac{L_s}{L_m}\left(\frac{P_{s\_dc\_ref}}{M_2}\begin{vmatrix} u_{sd+}^{+} \\ u_{sq+}^{+} \\ u_{sd-}^{-} \\ u_{sd-}^{-} \end{vmatrix} + \frac{Q_{s\_dc\_ref}}{M_1}\begin{vmatrix} u_{sq+}^{+} \\ -u_{sd+}^{+} \\ -u_{sq-}^{-} \\ u_{sd-}^{-} \end{vmatrix} \right) \tag{17}$$

where

$$M_1 = \left(u_{sd+}^{+\wedge 2} + u_{sq+}^{+\wedge 2}\right) - \left(u_{sd-}^{-\wedge 2} + u_{sq-}^{-\wedge 2}\right)$$
$$M_2 = \left(u_{sd+}^{+\wedge 2} + u_{sq+}^{+\wedge 2}\right) + \left(u_{sd-}^{-\wedge 2} + u_{sq-}^{-\wedge 2}\right)$$

c). Balanced stator active power (BSAP)

The references of active power oscillation terms are both set to zero, P_{s_dc} and Q_{s_dc} are set to their reference, and then the rotor reference currents can be obtained as,

$$\begin{vmatrix} i_{rd+}^{+} \\ i_{rq+}^{+} \\ i_{rd-}^{-} \\ i_{rq-}^{-} \end{vmatrix} = \frac{1}{\omega_s L_m}\begin{vmatrix} u_{sq+}^{+} \\ -u_{sd+}^{+} \\ -u_{sq-}^{-} \\ u_{sd-}^{-} \end{vmatrix} + \frac{2}{3}\frac{L_s}{L_m}\left(\frac{P_{s\_dc\_ref}}{M_1}\begin{vmatrix} u_{sd+}^{+} \\ u_{sq+}^{+} \\ -u_{sd-}^{-} \\ -u_{sd-}^{-} \end{vmatrix} + \frac{Q_{s\_dc\_ref}}{M_1}\begin{vmatrix} u_{sq+}^{+} \\ -u_{sd+}^{+} \\ u_{sq-}^{-} \\ -u_{sd-}^{-} \end{vmatrix} \right) \tag{18}$$

IV. Simulation Results

For the aforementioned three control targets, the DC-link capacitor current ripples are compared by the simulation results based on a 2MW DFIG Matlab/Simulink model, whose parameters are listed in TABLE II. In order to show the effects of the voltage negative sequence on the capacitors lifetime, a case with 3% negative sequence for a single-phase voltage unbalance is simulated.

TABLE II SIMULATION PARAMETERS OF 2MW DFIG STUDY CASE

Parameters		Values
Rate Power (MW)	P	2
Grid frequency (Hz)	f_g	50
Stator rated voltage (V)	V_S	690
Stator resistance (Ω)	R_s	0.0022
Rotor resistance (Ω)	R_r	0.0018
Stator inductance (mH)	L_s	3.012
Rotor inductance (mH)	L_r	2.95
Mutual inductance (mH)	L_m	2.9
Number of pole pairs	n_p	2
DC-link voltage (V)	V_{dc}	1200
DC-link capacitance (mF)	C_{dc}	22.5
Switching frequency (Hz)	f_c	5000

The simulation results are shown in Fig. 3. In Fig. 3(a), which is considered as the base case, the three-phase grid voltages are balanced, and, consequently, the DFIG exhibits best performances in terms of balanced stator active and reactive power, balanced electromagnetic torque and non-disturbed sinusoidal rotor currents. For the case of the considered voltage unbalance, the three rotor current control targets presented in Section III are adopted. The corresponding simulation results are shown in Fig. 3(b), (c) and (d), respectively. In Fig. 3(b), the three-phase rotor currents are controlled balanced, while the stator active and reactive power as well as electromagnetic torque all include oscillation terms. In Fig. 3(c), the stator reactive power and electromagnetic torque are balanced, while in Fig. 3(d) the stator active power is controlled balanced.

In order to compare the effects of different control targets on the DC-link capacitor lifetime, the capacitor current spectra presented in Fig. 4 are considered for the calculation of the capacitor hotspot temperature. In case of voltage unbalance, it

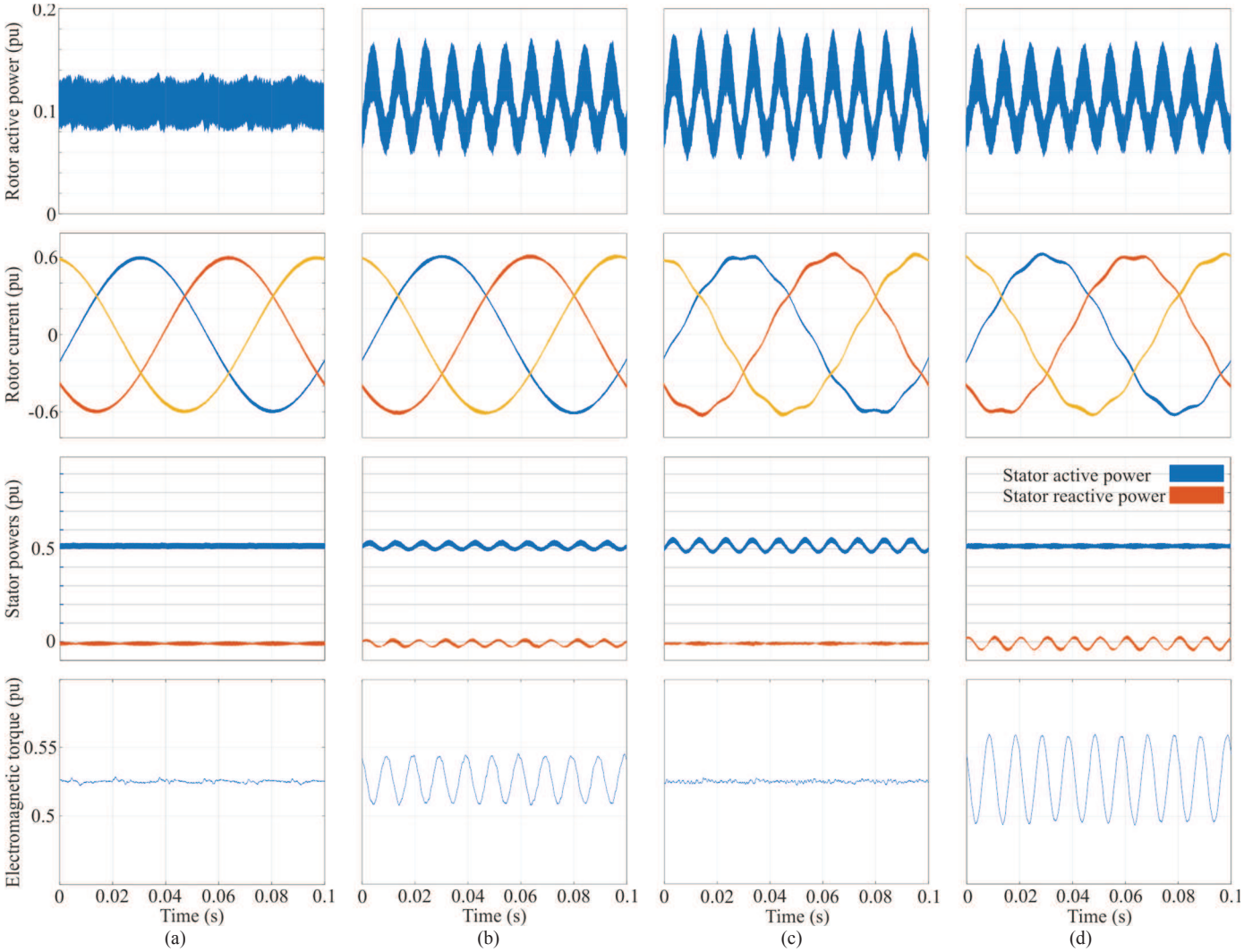

Fig. 3 Simulation results of 2MW with different control objectives: (a) Balanced grid voltage, normal rotor current control; (b) Balanced rotor current control; (c) Balanced stator reactive power and electromagnetic torque; (d) Balanced stator active power control.

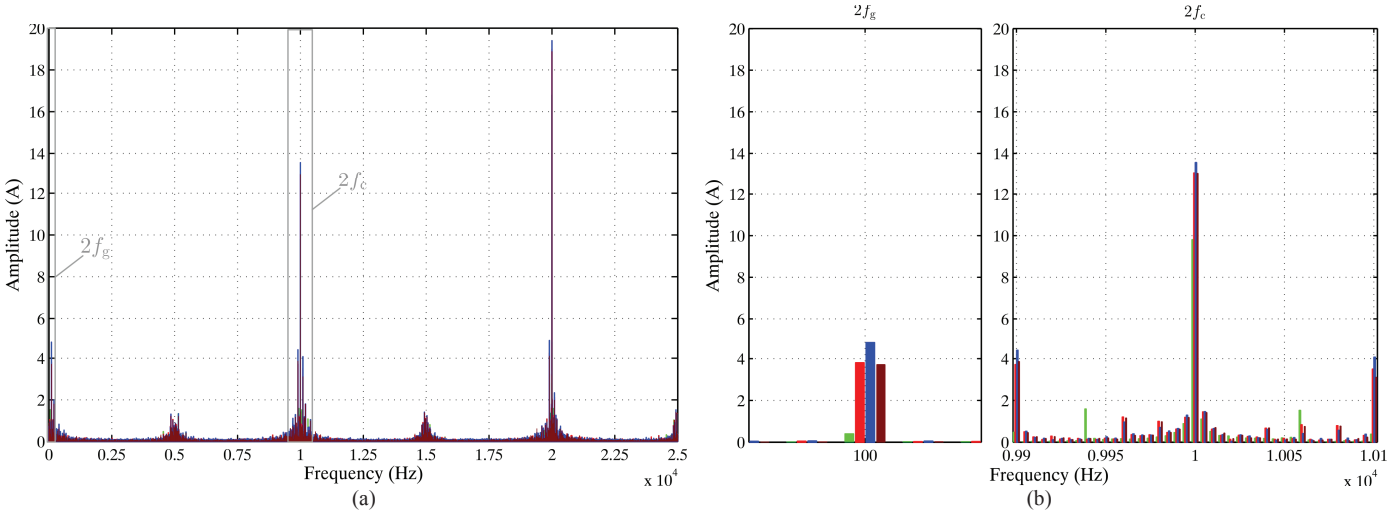

Fig. 4 Simulation results of single DC-link capacitor current spectrum (green: Base case, red: BRC, blue: BSRP, brown: BSAP): (a) Plot of the capacitor current spectrum up to $5f_c$; (b) Zoom into two exemplary frequency regions: $2f_g$ and $2f_c$.

is evident that the low frequency current ripple harmonics are significantly increased. Especially at 100 Hz high ripple current components are present, which is due to the oscillation of the rotor active power that results from the presence of negative sequence components in either rotor voltage or rotor current or in both signals, respectively.

In the following, the impact of the different rotor current control targets during grid voltage unbalance on the lifetime of a single DC-link capacitor is discussed. For this, it is assumed that the DC-link capacitor bank is configured from identical capacitors of the CUT type. In order to meet the DC-link voltage with a considerable safety margin, a series connection of three capacitors in a single branch is considered. Thus, for reaching a total capacitance of 22.5 mF a parallel connection of 15 capacitor branches is required. Hence, the current in a single branch is found to be the overall capacitor current divided by 15, given that all capacitors have identical electrical parameters. Accordingly, the current stress for a single DC-link capacitor is equal to this branch current. Based on this and the characteristics of the capacitor's ESR as discussed in Section II the losses of the CUT for the considered simulation cases are obtained. Afterwards, the hotspot temperature increase ΔT_h is calculated. In Table III an overview of the resulting changes in CUT RMS current I_{cap}, hotspot temperature increase ΔT_h, relative hotspot temperature increase with respect to the base case (balanced grid voltages) $\Delta T_{h,rel}$, and the relative lifetime in relation to the base case L_{rel} is provided.

TABLE III RESULTS FOR RELATIVE LIFETIME OF CUT FOR CONSIDERED SIMULATION CASES

Simulation case	**CUT RMS current I_{cap} (A)**	**Hotspot temperature increase ΔT_h (K)**	**Relative hotspot temperature change $\Delta T_{h,rel}$ (K)**	**Relative lifetime L_{rel} referred to base case (pu)**
Base case*	23.27	26.36	0.00	1
Balanced rotor currents	25.69	33.05	6.69	0.629
Balanced stator reactive power and electromagnetic torque	26.15	34.29	7.93	0.577
Balanced stator active power	25.62	32.87	6.51	0.637

*Balanced grid voltages

In case of balanced grid voltages, since it is considered as base case, $L_{rel} = 1$ and $\Delta T_{h,rel} = 0$ K are assumed. In the event of the considered grid voltage unbalance, the rotor currents are initially controlled to be balanced as shown in Fig. 3(b). As it is evident from the waveform of the rotor active power, the latter is oscillating at twice the grid frequency. Due to the additional low frequency ripple current components, and especially the 100 Hz component, the RMS current through the CUT and, subsequently, the capacitor losses are increased. This results in a relative hotspot temperature increase of $\Delta T_{h,rel}$ =6.69 K. Based on the considered lifetime model this temperature increase results in a relative lifetime of L_{rel} = 0.629 compared to the base case, being a significant lifetime reduction. If the rotor current is controlled such as to achieve constant stator reactive power and constant electromagnetic torque, the ripple current stress of the CUT is further increased. As can be seen in Fig. 3(c), the rotor active power exhibits a second order oscillation in this case and, in addition, the rotor currents are distorted by a negative sequence component of twice the grid frequency. This leads to an increase in relative hotspot temperature of the CUT of $\Delta T_{h,rel}$ = 7.93 K, resulting in a relative lifetime of L_{rel} = 0.577. In comparison with the balanced rotor current control, it is to be noted that the constant reactive power and electromagnetic torque control leads to further thermal stress for the CUT for the case of the same grid voltage unbalance. As a third rotor current control target, constant active power control is investigated as depicted in Fig. 3(d). In that case, as can be seen in the DC-link capacitor current spectrum in Fig. 4, the 100 Hz ripple current component is reduced with respect to the constant reactive power control. Accordingly, the RMS CUT current is lower. Compared to the case of balanced grid voltages, the relative hotspot temperature change is $\Delta T_{h,rel}$ = 6.51 K and, thus, the relative lifetime is decreased to L_{rel} = 0.637. By comparing the three considered rotor current control targets, it can be concluded that for the cases of balanced rotor current control and balanced stator active power control similar results are obtained, whereupon the impact of balanced stator active power control on the CUT lifetime is the least during the considered unbalanced grid voltage condition. Instead, the control of constant reactive power leads to the highest decrement in the lifetime of the CUT.

V. CONCLUSIONS

Power quality issues, such as voltage sags and unbalances, are expected to increase with the increasing amount of distributed renewable energy sources, such as wind power systems. Under unbalanced grid voltage conditions different dual-loop control targets can be applied for the rotor current control of DFIG based wind turbines in order to support the machine's and/or the grid's performance, respectively. As shown in this paper, depending on the control target, a different negative sequence component appears in rotor voltages and currents, resulting in different low-frequency components in the DC-link capacitor's ripple current spectrum. Based on the considered grid voltage unbalance scenario and the characteristics of its ESR, the relative lifetime of the employed DC-link electrolytic capacitor in the B2B converter of a 2 MW DFIG wind turbine is estimated. By this it is demonstrated that if the hotspot temperature increase due to the voltage unbalance condition is not considered during the design phase the expected capacitor lifetime is reduced significantly in dependence of the voltage unbalance and the applied rotor current control target.

ACKNOWLEDGMENT

The research leading to these results has received funding from the European Research Council under the European Union's Seventh Framework Programme (FP/2007-2013) / ERC Grant Agreement n. [616344] - HEART and was carried out within the framework of the "LIFE-WIND" project funded

by Gesellschaft für Klimaschutz Schleswig-Holstein GmbH (EKSH).

REFERENCES

[1] K. Fischer, T. Stalin, H. Ramberg, J. Wenske, G. Wetter, R. Karlsson, and T. Thiringer, "Field-experience based root-cause analysis of power-converter failure in wind turbines," *IEEE Trans*. *Power Electron*., vol. 30, no. 5, pp. 2481-2492, May 2015.

[2] H. Wang and F. Blaabjerg, "Reliability of capacitors for dc-link applications in power electronic converters-an overview," *IEEE Trans. Ind. Appl*., vol. 50, no. 5, pp. 3569-3578, Sept. 2014.

[3] Y. Yang, K. Ma, H. Wang, and F. Blaabjerg, "Instantaneous thermal modeling of the dc-link capacitor in photovoltaic systems," in *2015 IEEE Applied Power Electronics Conference and Exposition (APEC)*, Mar. 2015, pp. 2733-2739.

[4] M. L. Gasperi, "Life prediction modeling of bus capacitors in ac variable-frequency drives," *IEEE Trans. Ind. Appl*., vol. 41, no. 6, pp. 1430-1435, Nov. 2005.

[5] A. Albertsen, "Electrolytic capacitor lifetime estimation" [Online]. Available: http://jianghai-europe.com/wp-content/uploads/1-Jianghai-Europe-E-Cap-Lifetime-Estimation-long-AAL-2012-10-30.pdf

[6] X. Liang, "Emerging Power Quality Challenges Due to Integration of Renewable Energy Sources" *IEEE Trans. Ind. Appl*., vol. 53, no. 2, pp 855-866, Mar.-Apr. 2017.

[7] P. Cheng, H. Nian, C. Wu, Z. Q. Zhu, "Direct stator current vector control strategy of DFIG without phase-locked loop during network unbalance" *IEEE Trans. Power Electron*., vol. 32, no. 1, pp 284-297, Jan. 2017

[8] J. Hu, H. Xu, Y. He, "Coordinated control of DFIG's RSC and GSC under generalized unbalanced and distorted grid voltage conditions," *IEEE Trans., Ind. Electron.*, vol. 60, no. 7, pp 2808-2819, Jul. 2013

[9] R. Zhu, Z. Chen, X. Wu, and H. Liu, "High order sliding mode control of doubly-fed induction generator under unbalanced grid faults," in *IECON 2013-39th Annual Conference of the IEEE Ind. Electron. Society*, Nov. 2013, pp. 1662-1667.

[10] L. Xu, "Coordinated control of dfig's rotor and grid side converters during network unbalance," *IEEE Trans. Power Electron*., vol. 23, no. 3, pp. 1041-1049, May 2008.

[11] R. Zhu, Z. Chen, Y. Tang, F. Deng, and X. Wu, "Dual-loop control strategy for DFIG-based wind turbines under grid voltage disturbances," *IEEE Trans. Power Electron*, vol. 31, no. 3, pp. 2239-2253, Mar. 2016.

[12] H. Jedtberg, M. Langwasser, R. Zhu, G. Buticchi, T. Ebel, and M. Liserre, "Impacts of unbalanced grid voltages on lifetime of dc-link capacitors of back-to-back converters in wind turbines with doubly-fed induction generators," in *2017 IEEE Applied Power Electronics Conference and Exposition*, Mar. 2017, pp. 816-823